RC25497 (MRL1409-009) September 29, 2014
Chemistry

IBM Research Report

CO_2 and Air Nano-Bubbles Expansion and Dynamics on Amorphous Silica Surface

A. Bojovschi, Xi Liang, Sue A. Chen
IBM Research Division
204 Lygon Street
Carlton, Victoria 3053
Australia

Research Division
Almaden – Austin – Beijing – Cambridge – Dublin - Haifa – India – Melbourne - T.J. Watson – Tokyo - Zurich

CO_2 and air nano-bubbles expansion and dynamics on amorphous silica surface

A. Bojovschi, Xi Liang and Sue A. Chen

IBM Research – Australia, 204 Lygon Street, Carlton, Victoria 3053, Australia

ABSTRACT Nano-bubbles were shown to have numerous applications. Their modelling however, is largely limited to coarse grain methods. This work reports on the dynamics of CO_2 and air nano-bubbles on amorphous silica surfaces, immersed in water, using all-atom simulation. Most studies explore the formation and dynamics of nano-bubbles in gas supersaturated liquids. This study investigates the formation of nano-bubbles from high density molecular gase regions placed in solution. This allows us to examine the temporal expansion and stability of nano-bubbles. The expansion is accompanied by a decrease in density that is shown to follow an exponential decay. The stable value of the gas density in the nano-bubbles was attributed to a continuous diffusion of molecular gases. Thus accounting for the stability of nano-bubbles. During the equilibrium the contact angle between the nano-bubbles and silica surfaces are between about 15 and 25 degrees. The results are in agreement with theoretical and experimental studies that investigate nanobubbles.

1 To whom correspondence should be addressed: Electronic mail: alexe.bojovschi@au1.ibm.com

KEYWORDS nano-bubbles, CO_2, air, gas expansion, Molecular Dynamics (MD)

INTRODUCTION

The controversial existence of nano-bubbles driven by thermodynamic arguments deemed their existence impossible.[1-4] However, recent experimental, theoretical and computational studies provide enough evidence for their existence.[5-11] These studies brought fundamental insights related to spontaneous appearance of nano-bubbles at the interface between a liquid and a hydrophobic surface[5,12], the contribution to long range attraction forces and the role on the liquid slip and drag at the interface.[13-16] Increased understanding of nano-bubbles provided new avenues for their use in a wide range of industries such as flotation,[17-19,] water treatment,[20-21] biomedical engineering[22-25] and nano-materials.[26-28]

Molecular dynamics (MD)[29] is used extensively to study phenomena such as homogeneous and heterogeneous nucleations, explosive boiling and spinodal decomposition. The reason for the wide use of MD for these type of investigations is that the phase change is a non-equilibrium molecular dynamic (NEMD) process. Computational methods that address the characteristics of nano-bubbles explore nucleation, cavitation and stability.[30-36] A large amount of studies use MD to shed light on these phenomena in unary systems such as Ar, He, Pb, Li and Na. Lennard–Jones (LJ) pair potential is used in the majority of the investigations. For example the bubble nucleation rate explored in liquid Ar was carried out before.[32,34,36] Research that investigated the bubble dynamics in mixtures were carried out.[37-43] These studies included bubble nucleation in supercritical carbon dioxide–hexadecane, bubble nucleation and collapse in water as well as the effects of salts. Simulations of nano-cavity in chloride solutions with a non-polarizable force field have shown that the ions tend to resist the cavity collapse.[43] The ability of ions to create relative ordered structures in water can be estimated from the Hofmeister scale[45] which defines their kosmotrophic or chaotropic characteristics. MD studies revealed that nanobubbles appear in the form of the high density gas states at the water–graphite interface and in bulk water.[45,46] These works investigated the accumulation behavior of N_2 and H_2 at water graphite interface and in bulk water under ambient temperature and pressure. The authors pointed out that the extra high densities of the N_2 and H_2

molecules inside the gas pancakes and nano-bubbles are unexpected. Their results contradicted the conventional knowledge derived from the Young-Laplace equation. However, it has been argued that the large density supports understanding the stability of nano-bubbles.[47] Recent MD simulations of bubble coalescence included up to 38.4 billion Lennard-Jones particles.[48] This work sugessted that multiscale phenomena addressing phase transitions are feasible and that the molecular dynamics is a promising technique that can be applied to petascale computers.

The interactions between molecular gases such as N_2, O_2 and CO_2 and mineral surfaces are important in flotation, cleaning and CO_2 sequestration technologies. Silica (SiO_2) is the most common mineral on earth with a tetrahedral network structure in which silicon atoms are the centers of the tetrahedra with oxygen atoms acting as bridges between them. Theoretical and computational methods that predict the properties of silica were developed. Computational methods include various types such as *ab initio* type calculations[49-55] and Molecular Dynamics (MD).[56-65] Molecular simulation of the silica surface and their interaction with water or small molecules were reported in numerous studies.[66-72] The use of dehydroxylated/deprotonated and artificially hydroxylated/protonated amorphous silica surfaces were investigated.[66,72-74] MD simulations carried out by Leed and Pantano[72] were used to assess the adsorption of water on deprotonated and artificially hydroxylated surfaces. Results obtained by Bakaev and Steele, that used deprotonated silica surfaces, indicated that the surface defects and distortion of the SiO_4 tetrahedra as measured by their dipole and quadrupole moments give rise to hydrophilic adsorption sites on the surface.[48] These defects include 3-coordinated silicon and nonbridged oxygen (NBO) which contribute to the strong electrostatic field responsible for attractive forces. The study indicated that the irregularities of the amorphous silica surfaces and its roughness define its affinity for polar molecules. The role of surface topography and temperature on the substrate-fluid interaction strength were reported.[75]

To the best of our knowledge, the dynamics of nano-bubbles on a silica surface in solvent, at atomic level, has not been previously undertaken. In this study, we investigate using atomistic simulation the expansion, dynamics and stability of CO_2 and air nano-bubbles on an amorphous

silica surfaces in water. This work presents the dynamics of nano-bubbles on amorphous silica surface. This work is a first step towards tailoring their interactions using surfactants for mineral particle recovery in a flotation device.

MODELS AND METHODS

A. Modeling air and CO_2 on silica surface in solution

In this work, spherical volumes of high density CO_2 and air (N_2 and O_2) are placed at 0.3 nm away from the center of the amorphous silica surfaces and are fully solvated (Figure 1). The air mixture consists of 80% N_2 and 20% O_2. Other atoms and molecules commonly present in air, such as Ar, Ne, CO_2 and CH_4 are not considered due to their very low concentration and the small size of bubbles studied herein. A summary of the investigated systems with their gas phases including the number of atoms and molecules is presented in Table 1. The three dimensions in the Cartesian system of the dehydroxylated amorphous silica particle are x = 15.4981 nm, y = 15.499 nm and z = 20 nm. The initial dimensions of the two investigated systems are x = 15.4982 nm, y =15.499 nm and z = 15.998 nm. The initial state of the systems corresponds to a dense gas phase with all molecules situated in a sphere of 3 nm radius. The initial density of air was 0.052 a.u./Å^3 and of CO_2 was 0.109 a.u./Å^3. The solvent used in both systems (Figure 1) is water.

Our own routines programmed in Bourne Again Shell (BASH), Tool Command Language (TCL), Matrix Laboratory (MATLAB) and Visual Molecular Dynamics (VMD)[76] were employed to (a) build the simulated systems, (b) check for steric clashes, (c) analyze the simulation trajectory and (d) perform structural analyses. The amorphous silica layer was generated with the aid of InorganicBuilder within VMD. The tcl scripting interface in VMD was used to generate all the other components of the simulated systems. The representation and coloring method used for presenting atomic structure of CO_2, N_2, O_2 and SiO_2 is the Corey, Pauling and Koltun (CPK) space filling molecular model.[77] The CPK method renders the atoms as spheres with the size determined by the

van der Waals (vdW) radius. The surface rendering method, as implemented in VMD, was also used. The atom colours are depicted by the accepted color conventions for carbon (cyan), nitrogen (blue), silicon (yellow) and oxygen (red). The H_2O was rendered using a transparent surface (Figure 1) which allows the nano-bubbles to be visible.

B. Molecular simulation

Molecular dynamics (MD) was used in this work to characterize the dynamics of systems comprising of CO_2 and air, silica and water. All simulations were performed using NAMD 2.9[78] with the molecular constituents of the systems defined using CHARMM 22-27 (Chemistry at HARvard Molecular Mechanics) force field.[79] A list of gases and their parameters used is presented in Table 2. The TIP3P water model as optimized in CHARMM was adopted.[80] The force field of amorphous silica as available in CHARMM was used.[81] The amorphous silica layer was fixed during the simulations. All molecular systems were first minimized and then equilibrated using standard procedures.[82] The depth first search method implemented in NAMD was used to minimize the system. The systems were equilibrated using MD simulations that included constant temperature and pressure control via Langevin Dynamics (LD) and Nosé-Hoover Langevin piston pressure control. The LD temperature control, implemented in NAMD, consisted of adding a random force and subtracting a friction force from each atom during simulation to keep the temperature constant. The equilibrium was considered to be achieved when the density of nano-bubbles reached a plateau. An algorithm combining the Nosé-Hoover method[83] with the control fluctuations in the barostat implemented using Langevin dynamics[84] was employed to keep the pressure of the system constant. The velocity Verlet algorithm[85] was used to integrate the equations of motion. The cut-off distance was set to 14 Å for long range vdW interactions. A switching function of 12 Å was used to smoothly reduce the forces and energies to zero at the cut-off distance. The systems presented in this work were investigated with periodic boundary conditions (PBC). The simulations were performed for 20

ns. The size of initial simulation box was sufficiently large to allow the bubbles to expand without reaching the boundaries. MD simulations were run in an NPT ensemble for a total of 20 ns with a 1 fs steps after an energy minimization period of 1000 time steps. This work presents the results obtained at the temperature of 300 K and a pressure of 1.013 atm, which corresponds to the atmospheric pressure at sea level. The smooth particle-mesh Ewald (SPME) method[86] was used to handle electrostatic interactions. SPME employs B-spline function as the base function for interpolation. The use of B-spline functions reduces the number of Fast Fourier Transforms (FFTs) required by half compared to the original particle-mesh Ewald (PME) method.[87] A PME tolerance of 10^{-6} was used, the PME coefficient was equal to 0.219, and a 4^{th} order interpolation was used. The full long-range electrostatics via SPME were evaluated every 2 fs.

B. Properties characterisation parameters

Structural descriptors of nano-bubbles were determined from the atomic density profiles of the simulated systems in the orthogonal planes (Figure 2.) at different time steps of the simulation. Figure 2a presents representative orthogonal cross sections of the system depicting the atoms used to generate an atomic density representation. The density profiles were generated using VMD at a resolution of 1 Å. This method allows the monitoring of the dynamics of semi-principal axes *a*, *b* and *c*, of nano-bubbles (Figure 2), and their contact angle with the silica surfaces during the simulation. This was achieved using an image processing routine implemented in MATLAB. An illustration of the method involved is presented in Figure 3 and Figure 4. The MATLAB routine computes the tri-axial parameters and the contact angle using image processing methods.[88] In the pre-processing, the bubble image is converted to a gray-value image and resampled to 1/10 of the original size in both x and y directions to reduce the computation cost. The region grow method[89] employed uses 5 seeds which include the center point and 4 points located 10 pixels above, below, on the right and on the left of the center (Figure 3b). The bubble is assumed to be located

approximately at the center of the image. The region, with 5 initial seed points, is iteratively grown by first comparing all unallocated neighboring pixels and then selectively including relevant pixels to the current region. The difference between the intensity of the pixels and the mean value of the region is used as a measure of contrast. The pixel with the smallest difference is allocated to the bubble. The process terminates when the intensity difference between the region mean and new pixel become larger than a certain threshold. A morphological closing is then applied on the generated bubble mask to fill all holes and smooth the boundary. The contour of the bubble segmentation obtained is shown on Figure 3c. The bounding box of the bubble is computed as the minimum rectangle enclosing the bubble (Figure 4d). The next step involves computing the bubble centroid (as marked in red in Figure 4d). The equatorial and polar lines that intersect in the center of the bubble (Figure 4d) are used to compute the tri-axial parameters.

The procedure employed to calculate the contact angle involves the use of a line parallel to the silica surface which approximates a tangent line to the nano-bubble. The routine extracts the leftmost and rightmost points that are located both on the line and the bubble. Two curve intervals are then determined on the boundary of the bubble. With one starting from point L to the leftmost point (LM) and the other starting from point R, extending to the rightmost point (RM) of the bubble boundary. On each side, the points on the curves are connected with the corresponding L or R on the bubble surface. The smallest angle formed by the segment obtained by this procedure and the horizontal line is defined as the contact angle on that side. The contact angles between the bubbles and the silica surfaces were estimated by averaging 4 angles from two orthogonal planes of density profiles that are perpendicular to x and y axis respectively (Figure 2).

The density of gases in the nano-bubbles were estimated by using three spheres of 25 Å in radius that were used to sample the space within the nano-bubbles and the local densities. These local densities were then averaged to determine the molecular density in the nano-bubbles.

The diffusion coefficients of CO_2, O_2 and N_2 were calculated during the simulation time using the Diffusion Coefficient Tool available in VMD. The diffusion was computed for x, y and z space. A lag time from 10th frame to 3990th frame with a step of 10 and an analysis interval from 1st frame to 4000th frame with a step of 1 were used.

The radial distribution function (RDF) provides information on the internal structure of atomic and molecular systems. In this work, it is used to study the arrangement of gas molecules in the proximity of silica surface. It can be defined by the following equation:

$$g_{ij}(r) = \frac{< n_{ij}(r, r+\Delta r) >}{\rho_j 4\pi r^2 \Delta r} \quad (1)$$

where $< n_{ij}(r, r+\Delta r) >$ represents the total number of atoms of species j in a spherical shell between r and $r+\Delta r$ with the center corresponding with the center of atom i and ρ_j is the density of species j in the system. The RDF gives the probability of finding two species at a separation distance *r*.

The trajectories of gas molecules are investigated by quantifying the distance between the center of the nano-bubble and center of mass of the specific molecule at every simulation time step. The reference center of the nano-bubble is determined at the 20 ns time step. Gas molecules which were inside the bubbles, on their surfaces, in water, on silica surfaces and in the matrix structure of silica at 20 ns time step were used to track their trajectory during simulation.

RESULTS

Measurements of the equatorial and polar diameters during the evolution of the bubbles, summarised in Figure 5, provide information on their expansion time and dynamics. The tri-axial parameters start from a value of 3 nm for *a*, *b* and *c* and evolve to average values of about 9.5 nm for *a*, *b* and *c*. It should be noted that in Figure 5, the lines connecting the data points serve only as a guide for the eyes and do not represent the data. In Figure 5a the two equatorial diameters (ED1 and ED2) and the polar diameter (PD) are presented for the CO_2 bubble for representative simulation time steps. In Figure 5b the ED1, ED2 and PD are presented for the air bubble. The evolution of the

volume of nano-bubbles is presented also in Figure 5. Based on the data, the volumetric expansion can be approximated with a sigmoid of the form $y = a + (b-a)/(1 + exp((t-t_0)/\tau))$. The fitting parameters for the volume of CO_2 bubble are a = 434.151, b = 126.039, t_0 = 2.993 and τ = 0.607 while for the air bubble, these are a = 439.583, b = 149.493, t_0 = 1.752 and τ = 0.284. Figure 4a and 4b indicate that the equilibrium values of the volumes of air and CO_2 bubbles are about 450 nm^3. This is due to a higher solubility of CO_2 in water compared to air molecules and its higher affinity for amorphous silica. In this study, it was observed that CO_2 diffuses readily in the amorphous silicon matrix. The probability of O_2 diffusing outside of the air bubble is very low in this simulation.

The volumetric expansion of nano-bubbles leads to a density change. The decrease in density of CO_2 and air in the nano-bubbles is presented in Figure 6. The lines connecting the data points provide guides for the eyes and do not represent data. The decrease of CO_2 and air in the bubbles over the course of the simulation indicates that they reach a similar density of about 0.0025 a.u./$Å^3$ and 0.0020 a.u./$Å^3$ respectively at equilibrium (Figure 6). The CO_2 nano-bubble started from a higher density and reached equilibrium at about 10 ns time step. The air bubble, on the other hand, started from a density value lower than that of the CO_2 nano-bubble and reached equilibrium after about 5 ns. The first order exponential decay of the following form $y = a*exp(-t/\tau) + y_0$ can be used to estimate the decrease of CO_2 and air density in the bubbles. The fitting parameters are a = 0.011 , τ = 2.538 and y_0 = 0.003 for CO_2 and a = 0.012, τ = 0.986 and y_0 = 0.002 for air. The results, presented later in this work, show that the density of gas equilibrates due to the diffusion of gas molecules in and out the nano-bubble. This is in agreement with the reason for the existence and stability of nano-bubbles, explained previously by a theoretical model.[90]

The analysis of contact angles results show that after about 2.5 ns, their values are relatively stable with some fluctuation within the error bar (Figure 7). The error bar was derived by averaging

over 4 data points obtained as indicated in the method section. It should be noted that in Figure 7, the lines do not represent data but serve as guiding aids. The average values of the contact angle at equilibrium range from about 15 to 25 degrees. The variability of contact angles shown in Fig. 6 are due to the nano-scopic heterogeneities and topographical diversity of the amorphous silica surface. This may be caused by any rough surface. AFM techniques indicated that amorphous silica has a roughness which lies within the 0.3 nm to 0.6 nm interval.[91] In our study, the roughness of the silica surface is about 0.35 nm. It should be nothed that concentration will dictate the time of bubble collapse since highly supersaturated liquids have larger propensity to form and sustain nano-bubbles. The diffusion coefficients for the molecular gases (Figure 8) follow an exponential decay.

The RDF was determined for O_2-Si, N_2-Si and CO_2-Si pairs (Figure 9). The first peaks in Figure 9 show the probability of finding the gas molecules in the first neighbouring shell of Si. The results indicate that CO_2 has the highest probability of being in the proximity of Si followed by N_2 and O_2. One should be aware that the amplitudes of RDF are expected to be influenced by the number of molecules in the system. At about 4 Å, a peak is evident for O_2-Si, N_2-Si and CO_2-Si pairs. At about 6.3 Å, a second peak is evident for N_2-Si and CO_2-Si pairs. The peaks evident in the RDF at about 4 Å and at 6.3 Å show a relative degree of order in the system. At further distance, the order is smaller and RDF does not exhibit any peaks.

The trajectories of three representative gas molecules of CO_2, N_2 and O_2 situated inside the nano-bubbles, on their surface, in water on the surface of amorphous silica and within the matrix of amorphous silica at the end of the simulation are presented in Figure 10, 11, 12, 13 and 14 respectively. Each simulation time containing the coordinates of all atoms at a given time, was obtained every 5000 fs over the 20 ns simulation. Knowing that the largest tri-axial parameter has a maximum value of about 5.25 nm, the results presented in Figure 10 show that the molecules move mainly within the nano-bubble. The 1st CO_2 molecule in Figure 10a moves on the bubble surface and within its interior. In Figure 10a there are some evidently larger values for the 2nd CO_2 molecule

between about 2.5 ns (500 simulation state) and 15 ns (3000 simulation state) with maximum values close to 12 nm. These indicate that the CO_2 exited the bubble and diffused back in the bubble at about 15 ns. The trajectory of the 2nd CO_2 shows two peaks in the transitory at about 7 ns and 17 ns which indicate molecular diffusion. A similar trajectory which indicates diffusion in and out the nano-bubble is exhibited by the 1st and 2nd N_2 molecules (Figure 10b). The 3rd N_2 molecule is confined to move only within the nano-bubble. Among the O_2 molecules only the 2nd molecule exhibits a transitory diffusion outside the nano-bubble (Figure 10c). It should be noted that the last data point corresponds to the molecule inside the nano-bubble. The results for the case when gas molecules are on the surface of the bubble show also trajectories that highlight the diffusive process (Figure 11) which are more evident for N_2 and CO_2 molecules. In Figure 11a 1st, 2nd and 3rd molecules of CO_2 diffuse in and out of nano-bubbles during the simulation time. In Figure 11b it is noted that only the 1st and 3rd N_2 molecules show transitory diffusion outside the air bubble. From Figure 11c it can be seen that only 2nd and 3rd O_2 molecules diffuse briefly from nano-bubbles. The results in Figure 10 and 11 indicate that the gas molecules are inside the nano-bubble for the majority of the time. The trajectory of three distinct CO_2, O_2 and N_2 molecules situated outside the bubble at the end of simulation are presented in Figure 12. The trajectories of CO_2, N_2 and O_2 molecules in Figures 12a, 12b and 12c provide evidence for an ongoing diffusion process which persists until the end of the simulation. It can be noted that O_2 molecules exhibit significant fluctuations, reflected from the data presented in Figure 12c. Measurements of the distances between the centre of the nano-bubbles and representative gas molecules revealed different aspects pertaining to the diffusion of gas in and out of the bubbles and their dynamics.

The attachment of molecular gases to amorphous silica surface and their trajectory in its matrix were investigated. The results presented in Figures 13 and 14 show the trajectory of representative molecules that are on the surface of silica surface and within its matrix at 20 ns simulation time. In Figures 13a and 13b the CO_2 and N_2 molecules display diffusive dynamics

indicated above until they ultimately stabilise in the proximity of the silica surface. This is indicated by small fluctuations observed in the distance between the centre of the bubble and the respective molecule. There were no O_2 molecules identified on the surface of the silica surface at the end of the simulation. In Figure 14, the trajectory of the three representative CO_2 and N_2 molecules in the silica matrix is shown. The trajectories for the 1st and 3rd CO_2 molecules show their stability after diffusion in the amorphous silica. The 2nd CO_2 molecule indicates jumps from one location in the matrix to the next until it is stabilised. All three molecules of N_2 stabilise after they enter the matrix (Figure 14b) without evident jumps from one location to the next. In this case also the presence of O_2 was not identified in the amorphous silica surface at the end of the simulation.

CONCLUSIONS

The present work reported from an atomistic level the expansion and stability of nano-bubbles on a amorphous silica particle. The results provide the foundation for using these approaches to explore structural descriptors and dynamic characteristics of nano-bubbles. A method for precisely determining the structural parameters of nano-bubbles was introduced. The results showed the expansion of nano-bubble from a dense phase to an equilibrium phase. They indicated that this process involves a volumetric expansion and an exponential decay of gas density within the nano-bubbles. The contact angle between nano-bubbles and silica surface was found to be in the range from about 15 to 25 degrees. The scattered values of contact angle were shown to be caused by heterogeneities and topographical diversity of surfaces. The results indicated that the stability of nano-bubbles over the majority of the simulation time is due to diffusion of gas molecules in and out of the nano-bubbles. This mechanism that ensured the stability of nano-bubbles is in agreement with theoretical studies reported before. Further work could involve the use of tailored surfactants to increase the attachment of the nano-bubbles to the silica surface.

ACKNOWLEDGEMENT

We thank the IBM Watson BlueGene/Q team for technical support and for generous allocation of computing resources. The constructive discussions and comments provided by Dr. George Yiapanis and Dr. Matthew Downton are also acknowledged.

REFERENCES

(1) Eriksson, J. C.; Ljunggren, S. Colloids Surf., A **1999**, 159, 159–163.

(2) Christenson, H. K.; Claesson, P. M. Adv. Colloid Interface Sci. **2001**, 91, 391-436.

(3) Attard, P. Adv. Colloid Interface Sci. **2003**, 104, 75-91.

(4) Ball, P. Nature **2003**, 423, 25-26.

(5) Seddon, J. R. T.; Lohse, D. J. of Phys: Cond. Matter **2011**, 23, 133001-133023.

(6) Wang Y.; Bhushan B. Soft Matter **2010**, 6, 29-66.

(7) Steitz, R.; Gutberlet, T.; Hauss, T.; Klosgen, B.; Krastev, R.; Schemmel, S.; Simonsen, A. C.; Findenegg, G. H. Langmuir **2003**, 19, 2409-2418.

(8) Switkes, M.; Ruberti, J. W., Appl. Phys. Lett. **2004** 84, 4759-4761.

(9) Poynor, A.; Hong, L.; Robinson, I. K.; Granick, S.; Zhang, Z.; Fenter, P. A. Phys. Rev. Lett. **2006**, **97**, 266101-266104.

(10) Zhang, X. H.; Khan, A.; Ducker, W. A. Phys. Rev. Lett. **2007**, 98, 136101-136104.

(11) Karpitschka, S.; Dietrich, E.; Seddon, J. R. T.; Zandvliet, H. J. W.; Lohse, D.; Riegler, H. Phys. Rev. Lett. **2012**, 109, 066102-066106.

(12) Craig, V. S. J. Soft Matter **2011**, 7, 40-47

(13) Tyrrell, J. W. G.; Attard, P. Phys. Rev. Lett. **2001**, 87, 176104-176107.

(14) de Gennes, P. G. Langmuir **2002**, 18, 3413-3414.

(15) Lauga, E.; Brenner, M. P. Phys. Rev. E **2004**, 70, 026311-026317.

(16) Maali, A.; Bhushan, B. J. Phys.: Condens. Matter **2013**, 25, 184003-184014.

(17) Fan, M.; Tao, D. Separation and Sci. Tech. **2008**, 43, 1-10.

(18) Tao, D. Separation Sci. Tech. **2010**, 39, 741-760.

(19)Kohama, Y.; Kukizaki, M.; Nakashima, T. Patent US 7,591,452 B2

, **2009**.

(20) Ashutosh, A.; Wun J. N.; Yu L. Chemosphere, **2011**, 84, 1175-1180.

(21) Spears, J. R.; Ridgway, J. W. Patent US 8,500,104 B2, **2013**.

(22) Lukianova-Hleb, E. Y.; Campbell, K. M.; Constantinou, P. E.; Braam J.; Olson J. S.; Ware, R.E.; Sullivan, D. J.; Lapotko, D. O. Proc. Natl. Acad. Sci. U S A, **2014**, 111, 900-905

(23) Lapotko, D.; Hleb, K.; Braam, J.; Olson, J. S. Patent WO2013109722, **2013**.

(24) Wagner, D.S.; Delk, N. A.; Lukianova-Hleb, E.Y.; Hafner, J. H.; Farach-Carson, M. C.; Lapotko, D.O. Biomaterials, **2010**, 31, 7567-7574.

(25) Lukianova-Hleb, E.; Koneva, I.; Oginsky, A.; La Francesca, S.; Lapotko, D. O. J Surg. Res., **2011**, 166, e3-13.

(26) Shen, G.; Zhang, H. X.; Ming, Y.; Zhang, L.; Zhang, Y.; Hu, J. J. Phys. Chem. C, **2008**, 112, 4029–4032.

(27) Santo, K. P.; Berkowitz, M. L. J. Phys. Chem. B, **2013**, 117, 5031–5042.

(28) Liu, G.; Wu, Z.; Craig, V. J. of Phys. Chem. C, **2008**, 112, 16748-16753.

Häbich, A.; Ducker, W.; Dunstan D. E.; Zhang, X. J. Phys. Chem. B, **2010**, 114, 6962–6967.

(29) Sadus. J. R. Molecular Simulation of Fluids, Elsevier, 2002.

(31) Park, S.; Weng, J. G.; Tien, C. L. Microscale Thermophys. Eng. **2000**, 4, 161–175.

(32) Wu, Y. W.; Pan, C. Microscale Thermophys. Eng. **2003**, 7, 137–151.

(33) Shekhar, A.; Ken-ichi, N.; Kalia, R. K.; Nakano, A.; Vashishta, P. Phys. Rev. Lett. **2013**, 111, 184503-184503.

(34) Neimark, A. V.; Vishnyakov, A. J. Chem. Phys. **2005**, 122, 054707-054716.

(34) Okumura, H.; Ito, N. Phys. Rev. E **2003**, 67, 045301-045304.

(35) Tsuda, S.-I.; Hirata, T.; Tanaka, H. Mol. Sim. **2013**, 40, 320-326.

(36) Nagayama, G.; Tsuruta, T.; Cheng, P. Int. J. of Heat and Mass Transfer **2006**, 49, 4437–4443.

(37) Tsuda, S. I.; Tokumasu, T.; Kamijo, K. Heat Transfer - Asian Research **2005**, 34, 514–526.

(38) Zhai, M.; Zhang, R. Z.; Li, Q.; Shen, C. Journal of Plastic Film and Sheeting, **2011**, 27, 117–126.

(39) Mao, Y.; Zhang, Y., Nanoscale and Microscale Thermophys. Eng. **2013**, 17, 79–91.

(40) Mark, P.; Nilsson L., J. of Comp. Chem. **2002**, 23, 1211–1219.

(42) Yamamoto, T.; Ohnishi, S. Phys. Chem. Chem. Phys. **2011**, 13, 16142–16145.

(43) Lugli, F.; Zerbetto, F. Chem. Phys. Chem. **2007**, 8, 47–49.

(44) Hofmeister, F. Arch. Exp. Pathol. Pharmacol. **1888**, 24, 247-260.

(45) Chun-Lei, W.; Zhao-Xia, L.; Jing-Yuan, L.; Peng, X.; Jun H.; Hai-Ping, F. Chin. Phys. B **2008**, 17, 2646-2654.

(46) Fang, H. P.; Hu, J. Nucl. Sci. Tech. **2006**, 17, 71－77.

(47) Borkent, B. M.; Dammer, S. M.; Schönherr, H.; Vancso G. J.; Lohse, D. Phys. Rev. Lett. **2008**, 98, 204502-204505.

(48) Watanabe H.; Suzuki, M.; Ito, N. Comput. Phys. Commun. **2013**, 184, 2775-2784.

(49) Michalske, T. A.; Bunker, B. C. J. Appl. Phys. **1984**, 56, 2686-2693.

(50) Kudo, F.; Nagase, S. J. Am. Chem. Soc. **1985**, 107, 2589-2595.

(51) O'Keeffe, M.; Gibbs, G. V. J. Phys. Chem. **1985**, 89, 4574-4577.

(52) Hammann, D. R. Phys. Rev. B **1997**, 55, 14784-14793.

(53) Ceresoli, D.; Bernasconi, M.; Iarlori, S.; Parrinello, M.; Tosatti, E. Phys. Rev. Lett. **2000**, 84, 3887-3890.

(54) Lopez, N.; Vitiello, M.; Illas, F.; Pacchioni, G. J. Non-Cryst. Solids **2000**, 271, 56-63.

(55) Vitiello, M.; Lopez, N.; Illas, F.; Pacchioni G. J. Phys. Chem. A **2000**, 104, 4674-4684.

(56) Carré, A.; Berthier, L.; Horbach, J.; Ispas, S.; Kob, W. J. Chem. Phys. **2007**, 127, 114512-114521.

(57) Horbach, J.; Kob, W.; Binder, K. J. Phys. Chem. B **1999**, 103, 4104-4108.

(58) Benoit, M.; Ispas, S.; Jund, P.; Jullien, R. Eur. Phys. J. B **2000**, 13, 631-636.

(59) Roder, A.; Kob, W.; Binder, K. J. Chem. Phys. **2001**, 114, 7602-7614.

(60) Herzbach, D.; Binder, K.; Müser, M. H. J. Chem. Phys. **2005**, 123, 124711-124721.

(61) Kerrache, A.; Teboul, V.; Monteil, A. Chem. Phys. **2006**, 321, 69-74.

(62) Léonforte, F.; Tanguy, A.; Wittmer, J. P.; Barrat, J.-L. Phys. Rev. Lett. **2006**, 97, 055501-055504.

(63) Berthier, L.; Biroli, G.; Bouchaud, J.-P.; Kob, W.; Miyazaki, K.; Reichman, D. J. Chem. Phys. **2007**, 126, 184504-184525.

(64) Cruz-Chu, E. R.; Aksimentiev, A.; Schulten, K. J. Phys. Chem. B, **2006**, 110, 21497–21508.

(65) Bakaev, V. A. Phys. Rev. B **1999**, 60, 10723-10726.

(66) Bakaev, V. A.; Steele, W. A. J. Chem. Phys. **1999**, 111, 9803-9812.

(67) Beckers, J. V. L.; de Leeuw, S. W.J. Non-Cryst. Solids **2000**, 261, 87-100.

(68) Bakaev, V. A.; Steele, W. A.; Bakaeva, T. I.; Pantano, C. G. J. Chem. Phys. **1999**, 111, 9813-9821.

(69) Mischler, C.; Horbach, J.; Kob W.; Binder K., J. Phys.: Condens. Matter **2005**, 17, 4005-4013.

(70) Chai, J.; Liu, S.; Yang, X. App. Surf. Sci. **2009**, 255, 9078-9084.

(71) Yiapanis, G.; Henry, D. J.; Maclaughlin, S.; Evans, E.; Yarovsky, I. Langmuir, **2012**, 28, 17263-17272.

(72) Leed, E. A.; Pantano, C. G. J. Non-Cryst. Solids **2003**, 325, 48-59.

(73) Yang, X.; Xu, Z.; Zhang, C. J. Colloid and Interf. Sci. **2006**, 297, 33-44.

(74) Stallons, J. M.; Iglesia, E. Chem. Eng. Sci. **2001**, 56, 4205-4216.

(75) Leroy, F.; Müller-Plathe, F. J. Chem. Phys. **2010**, 133, 044110-044121.

(76) Humphrey, W.; Dalke, A.; Schulten, K. J. Mol. Graph. **1996**, 14, 33-38.

(77) Corey R. B.; Pauling L. Rev. of Scientific Instruments **1953**, 24, 621-627

(78) Phillips, J. C.; Braun, R.; Wang, W.; Gumbart, J.; Tajkhorshid, E.; Villa, E.; Chipot, C.; Skeel, R. D.; Kale, L.; Schulten, K. J. Comput. Chem. **2005**, 26, 1781-1802.

(79) MacKerell, A. D.; Bashford, D.; Bellott, M.; Dunbrack, R. L.; Evanseck, J. D.; Field, M. J.; Fischer, S.; Gao, J.; Guo, H.; Ha, S.; Joseph-McCarthy, D.; Kuchnir, L.; Kuczera, K.; Lau, F. T. K.; Mattos, C.; Michnick, S.; Ngo, T.; Nguyen, D. T.; Prodhom, B.; Reiher, W. E.; Roux, B.; Schlenkrich, M.; Smith, J. C.; Stote, R.; Straub, J.; Watanabe, M.; Wiorkiewicz-Kuczera, J.; Yin, D.

; Karplus, M. J. Phys. Chem. B **1998**, 102, 3586-3616; Foloppe, N. and MacKerell, A. D. J. Comput. Chem. **2000**, 21, 86-104.

(80) Jorgensen, W. L. J. Am. Chem. Soc. **1981**, 103, 335-340.

(81) Cruz-Chu, E. R.; Aksimentiev, A.; Schulten, K. J. Phys. Chem. **2006**, 110, 21497-21508.

(82) Bojovschi, A.; Liu, M. S.; Sadus, R. J. J. Chem. Phys. **2012**, 137, 075101-075121.

(83) Martyna, G. J.; Tobias, D. J.; Klein, M. L. J. Chem. Phys **1994**, 101, 4177-4189.

(84) Feller, S. E.; Zhang, Y.; Pastor, R. W.; Brooks B. R., J. Chem. Phys. **1995**, 103, 10267-10276.

(85) Swope, W. C.; Andersen, H. C.; Berens, P. H.; Wilson, K. R. J. Chem. Phys. **1982**, 76, 637-649.

(86) Essmann, U.; Perera, L.; Berkowitz, M. L.; Darden, T.; Lee, H.; Pedersen, L. G. J. Chem. Phys. **1995**, 103, 8577-8593.

(87) Darden, T.; York, D.; Pedersen, L. J. Chem. Phys. **1993**, 98, 10089-10092.

(88) http://www.mathworks.com.au/products/image/

(89) Petrou M.; Bosdogianni, P. Image Processing the Fundamentals, Wiley, UK, **2004**

(90) Weijs, J. H.; Lohse, D. Phys. Rev. Lett, **2013**, 110, 054501-054506.

(92) Gupta, P. K.; Inniss D.; Kurkjian C. R.; Zhong Q. J Non-Cryst. Solids **2000**, 262, 200-206.

Table I. Summary of gases in pure water carried out in this work at 300K using an integration time step of 1fs.

System	Number of atoms	Number of N2	Number of O2	Number of CO2
SiO_2 CO_2 and H_2O	340551	-	-	489
SiO_2, O_2, N_2 and H_2O	339804	288	72	-

Table II. CHARMM parameters for N_2, O_2 and CO_2 used in this work.

	Specific charge	Bond length (Å)	Bond constant (kcal/mole/A^2)	σ(Å)	ε(kcal/mol)
CO2					
C	0.6			-0.06	1.56
CO1	-0.3			1.69	-0.17
CO2	-0.3			1.69	-0.17
C-CO1		1.16	937.96		
N2					
N	0			1.65	-0.2
N	0			1.65	-0.2
N-N		1.1	1007		
O2					
O	0			1.77	-0.15
O	0			1.77	-0.15
O-O		1.28	1180		

FIGURES

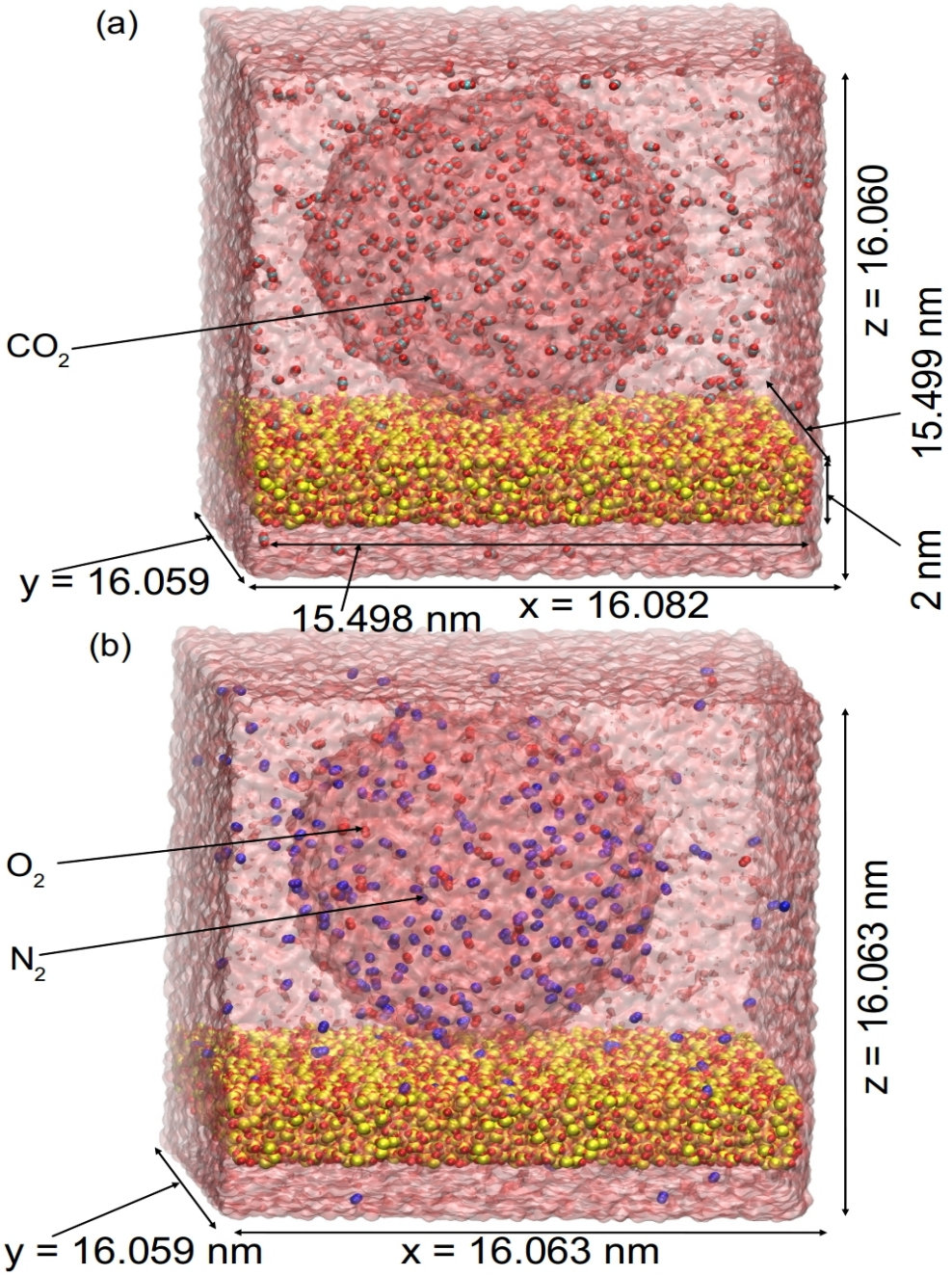

Figure 1. The simulation systems at 20 ns. The system consist of a) CO_2 and b) air bubble (N_2 and O_2) on the surface of amorphous silica immersed in water. The gas molecules and the silica layer are represented using van der Waals spheres. The water is rendered using a transparent surface.

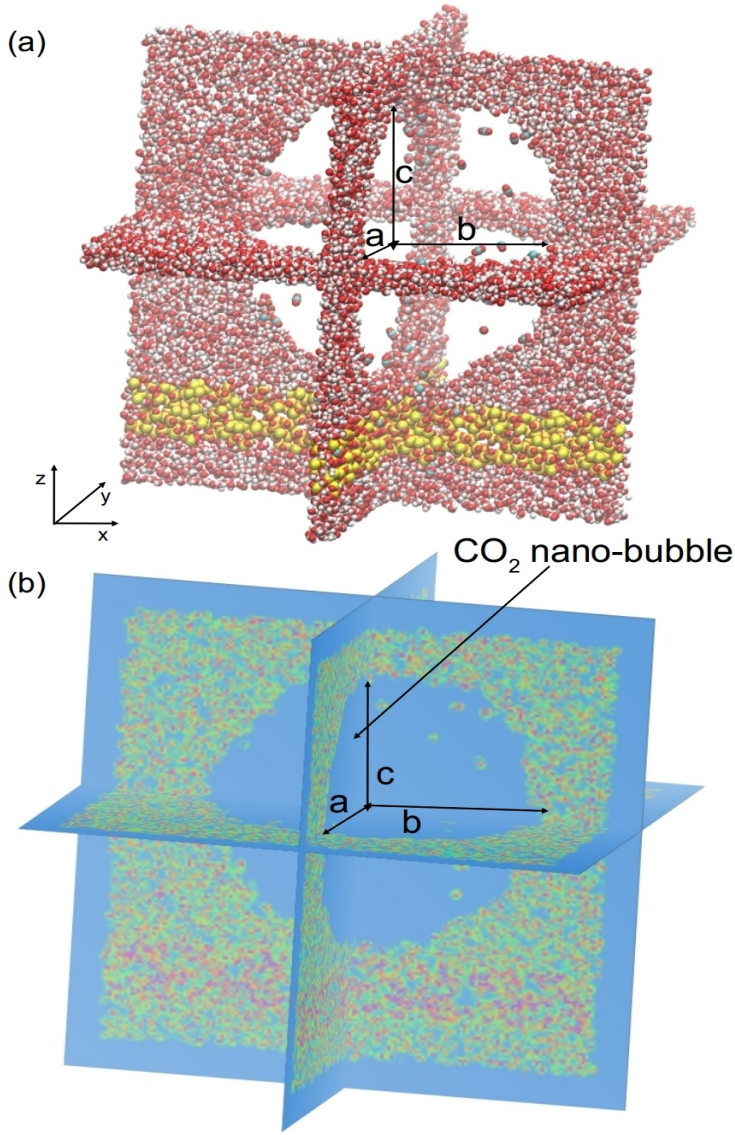

Figure 2. Representative view of a) three slices through the simulation system used to compute the density profile. Each slice has a thickness of 6 Å . Atomic density profiles b) of the orthogonal planes intersecting in the center of the gas bubble. The semi-principal axes *a*, *b* and *c* of the tri-axial ellipsoid used to derive the nano-bubble volume. The blue areas represent empty space while the other color zones indicate the presence of atoms. The descending atomic density is represented by colours that starts from dark red followed by orange, yellow, green and ends at blue. The details are resolved at 1 Å resolution.

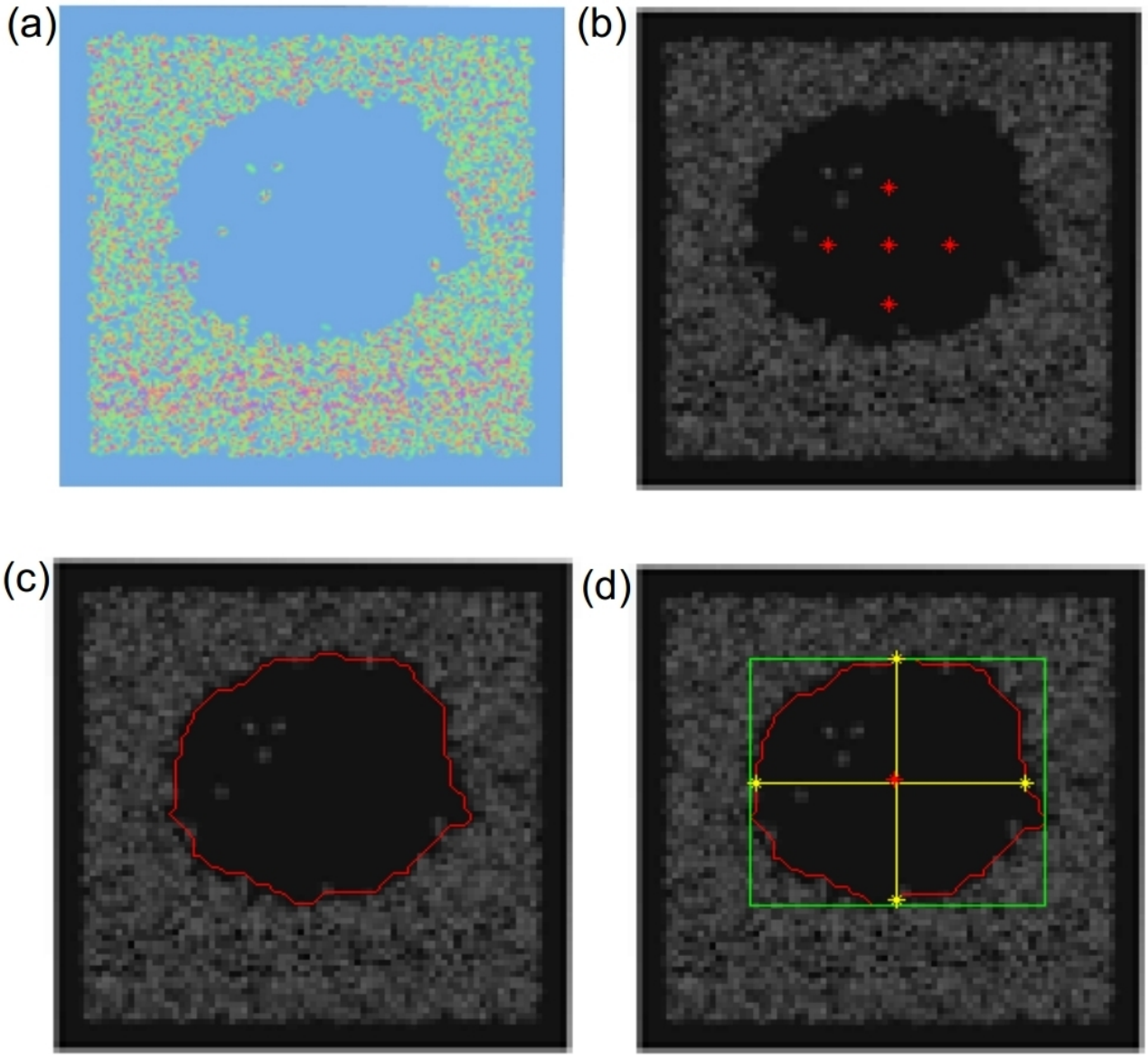

Figure 3. Steps employed for image processing analysis of the nano-bubbles density profiles to extract the tri-axial parameters. (a) Density profile of the cross section through the nano-bubble (b) 5 seeds points on gray-value image of the bubble. (c) Red contour of the region (nano-bubble) obtained by growing through segmentation using the 5 seed points. (d) Green bounding box of the bubble. The centroid is marked in red. The horizontal and vertical axis intersecting in the centre of the region of interest is colored in yellow.

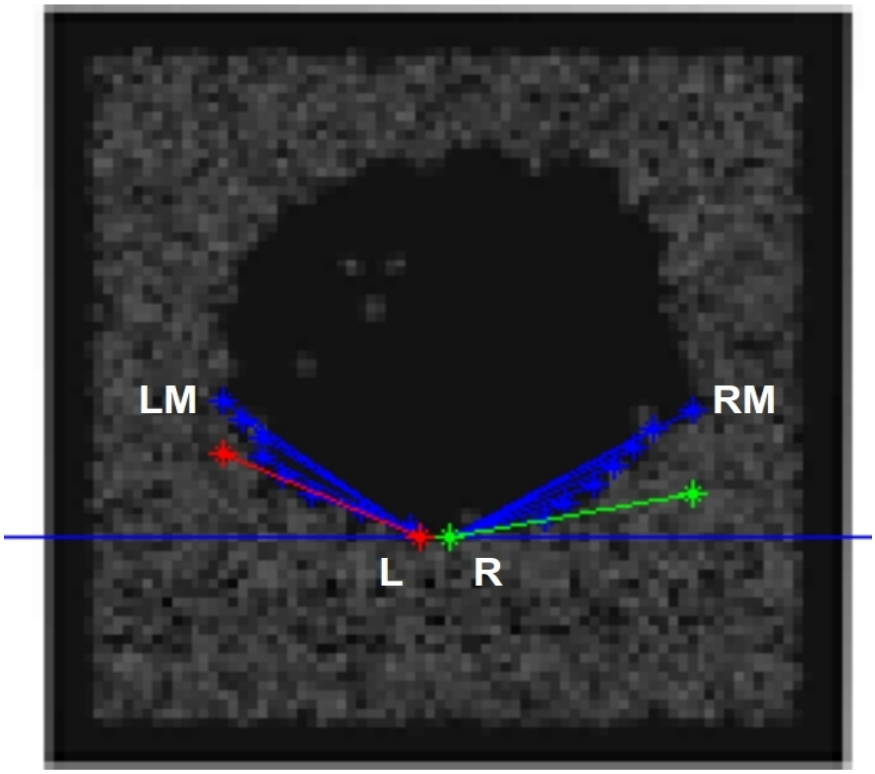

Figure 4. Procedure used to compute the contact angle. The left (in red) and right (in green) lines and horizontal tangent line were used to compute the contact angle.

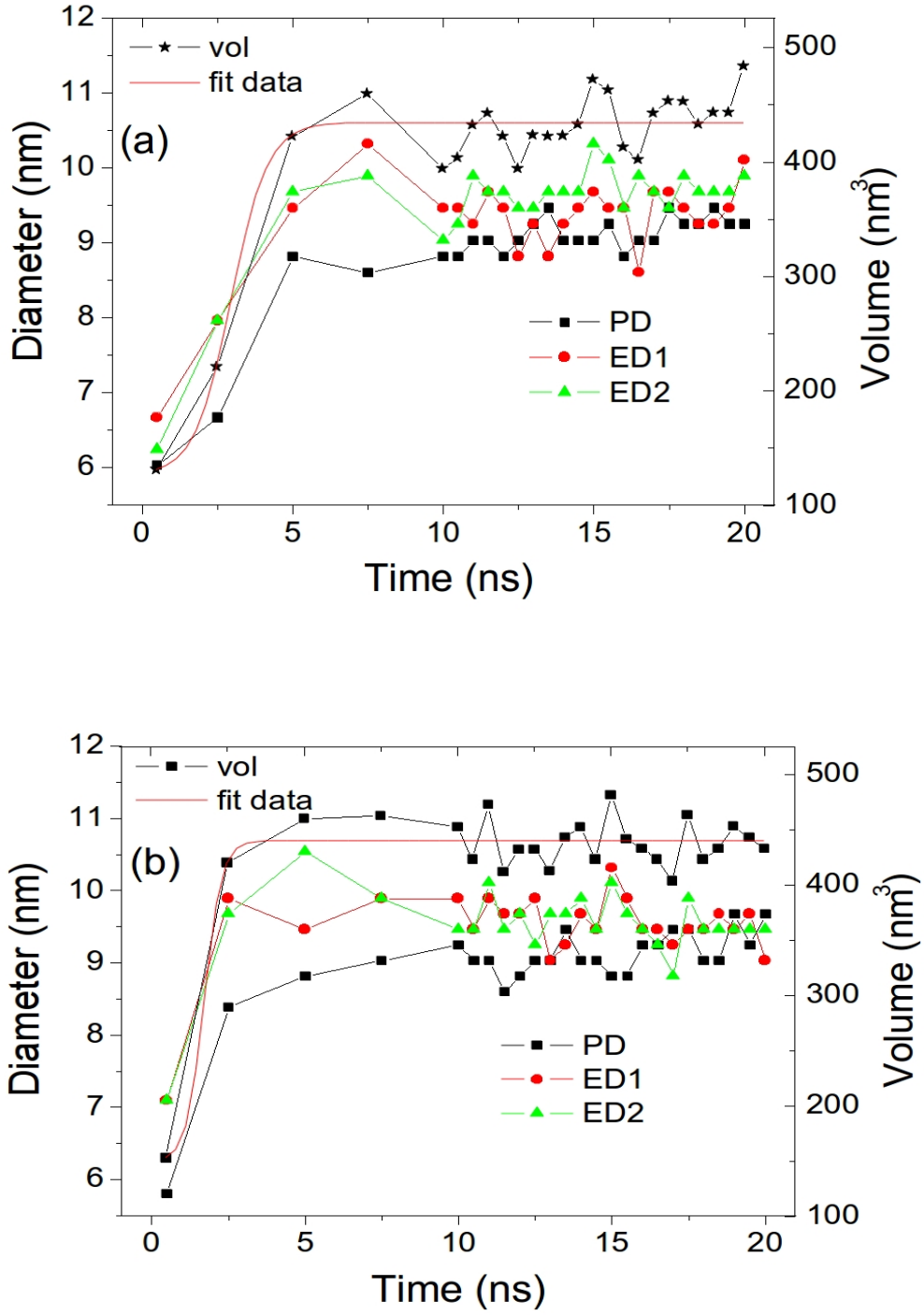

Figure 5. Geometrical descriptors of the bubbles. These include the equatorial diameters (ED1 and ED2), polar diameter (PD) and the volume (vol) of the tri-axial ellipsoid used to approximate the CO_2 (a) and air (b) bubbles. The volumetric expansion of CO2 and air bubbles over the simulation can be approximated by a sigmoid (fit data).

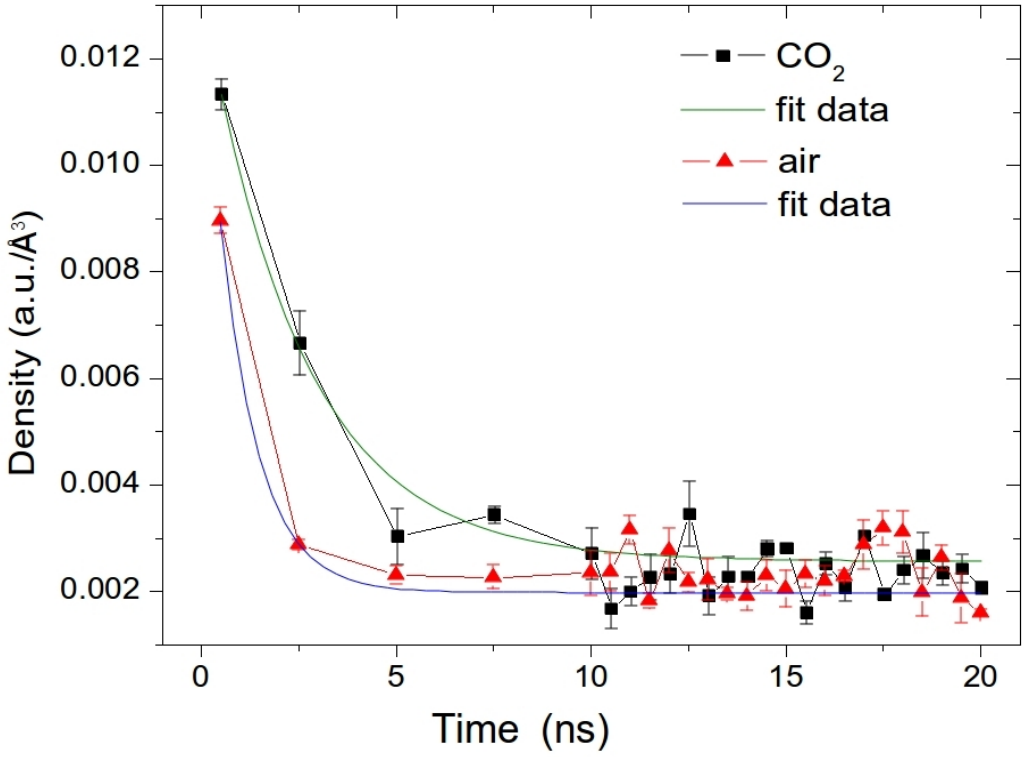

Figure 6. The time dependent density of the CO2 and air in the nano-bubbles. The data is averaged from three values obtained in three regions of the bubbles that sample the nano-bubble volume. The regions were defined by spheres of radius equal to 2.5 nm. The densities over the simulation time follow a first order exponential decay (fit data).

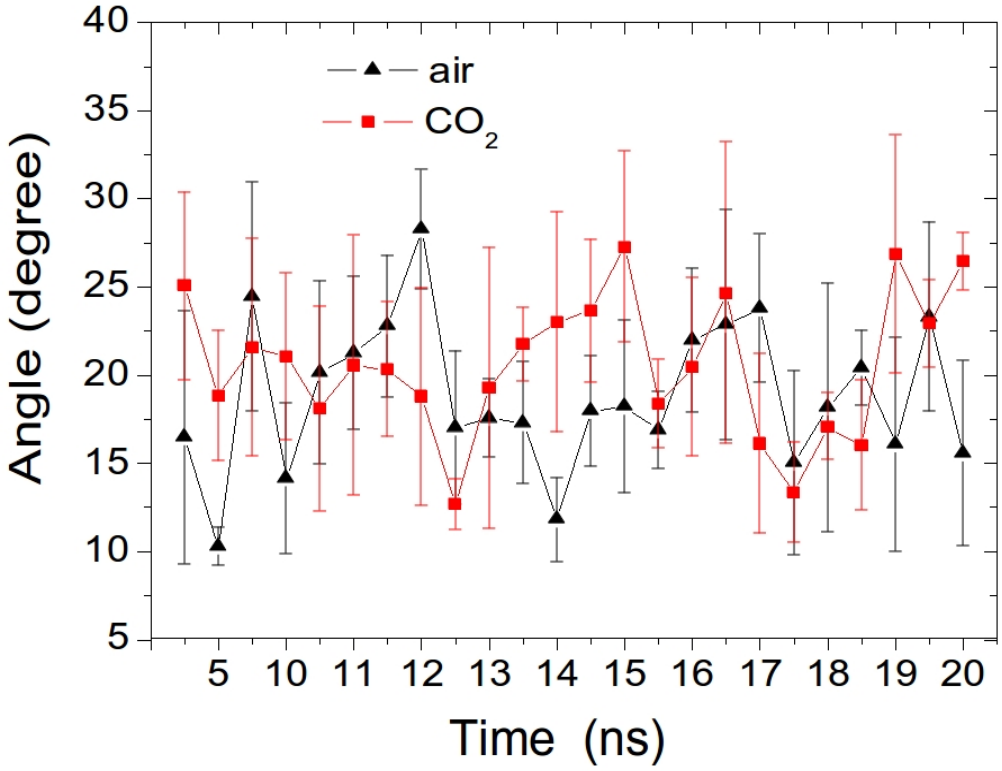

Figure 7. Contact angle between the air and CO_2 nano-bubbles and the amorphous silica surface. Eight values were collected to average the contact angle at each time step. The values of the contact angle were obtained using the method presented in Figure 3 whereby two orthogonal planes, perpendicular to x and y axes (Figure 2), of atom density profiles were use.

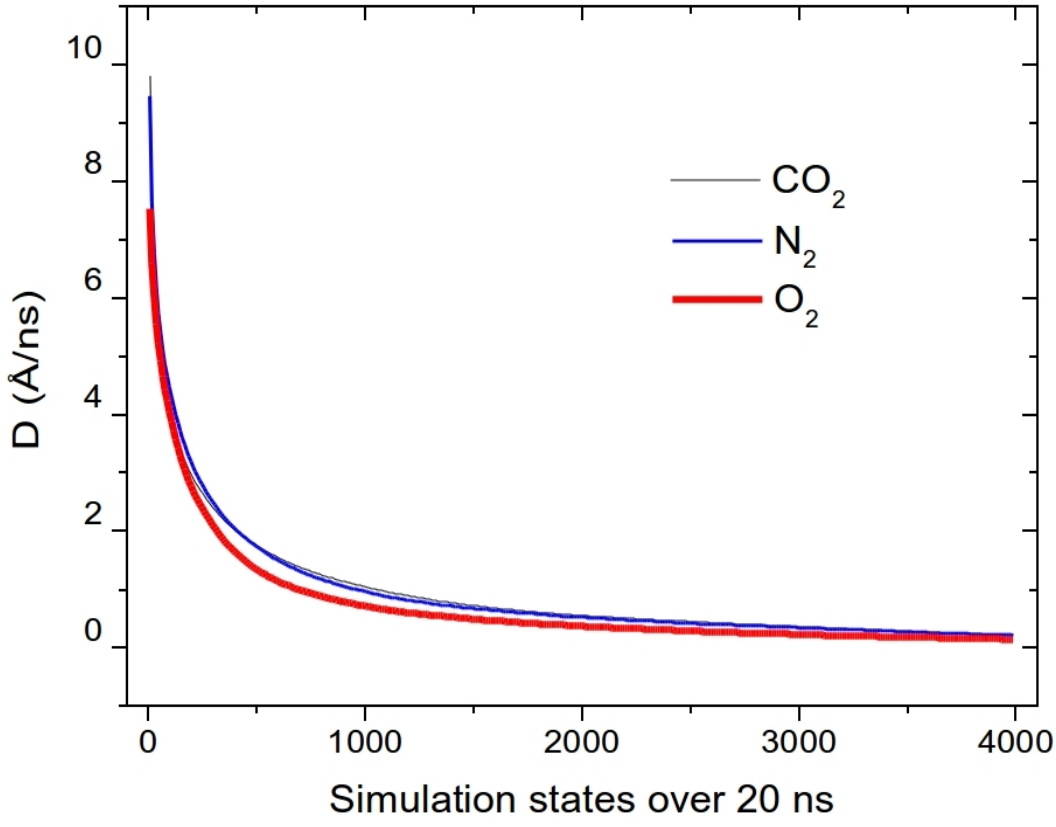

Figure 8. The diffusion coefficient of molecular gases (CO_2, N_2 and O_2) in the systems investigated over the simulation time.

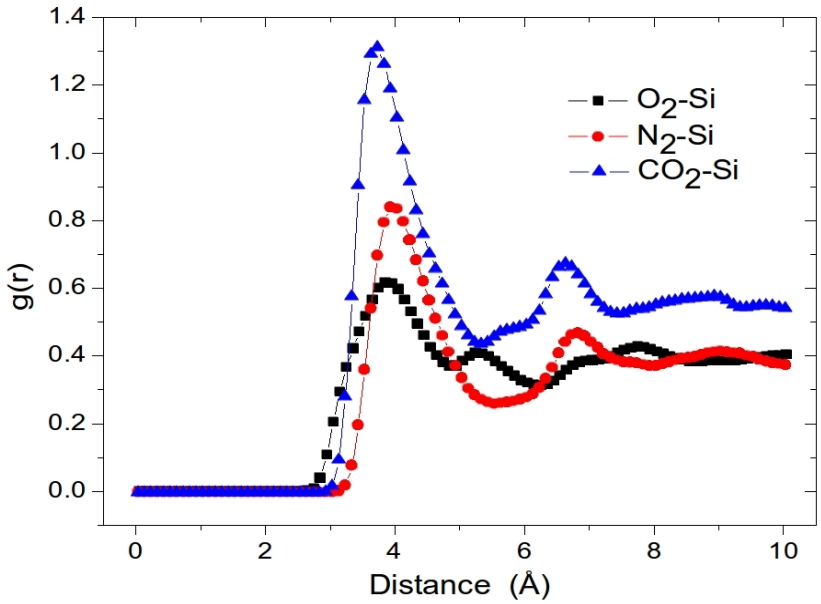

Figure 9. The RDFs for O_2-Si, N_2-Si and CO_2-Si obtained from the last 17.5 ns of the simulated systems.

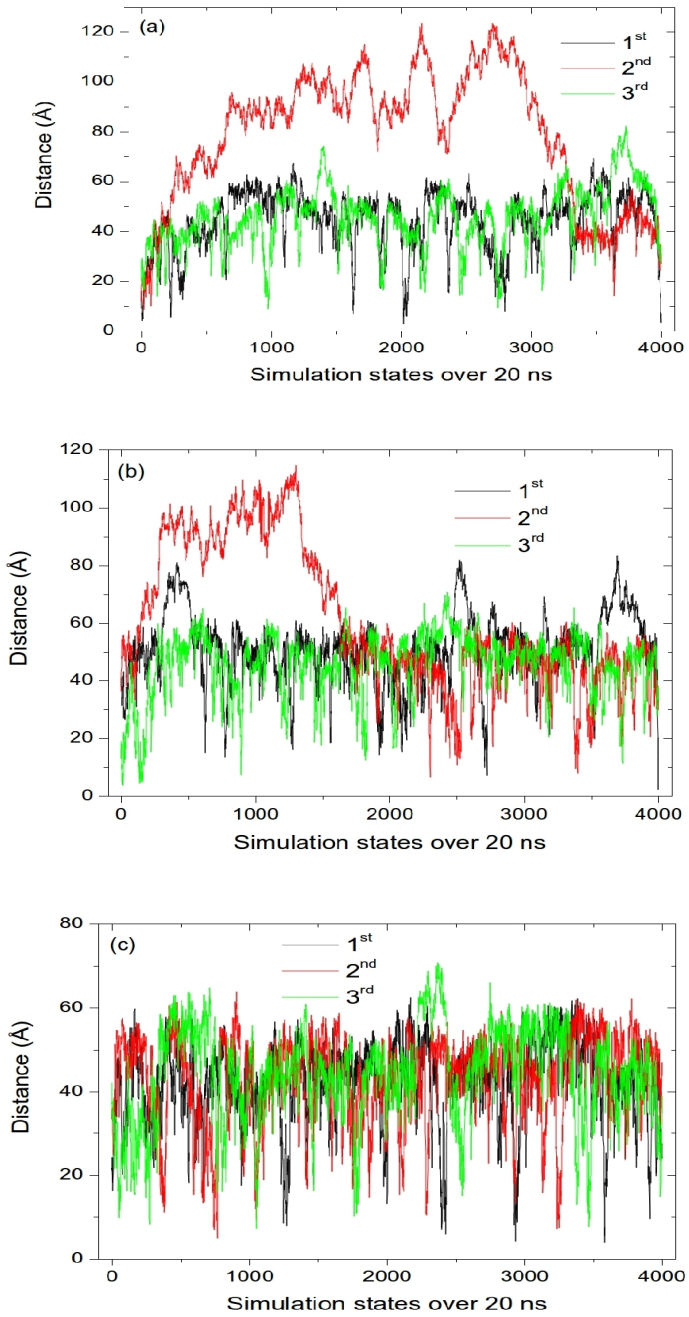

Figure 10. Representative dynamic displacement of CO_2 (a), N_2 (b) and O2 (c) molecules during the simulation time that are inside the nano-bubbles at the end of the simulation. The displacement was computed with reference to the centre of the bubbles estimated at 20 ns time step. The three data sets in each plot (1^{st}, 2^{nd} and 3^{rd}) correspond to three distinct gas molecules.

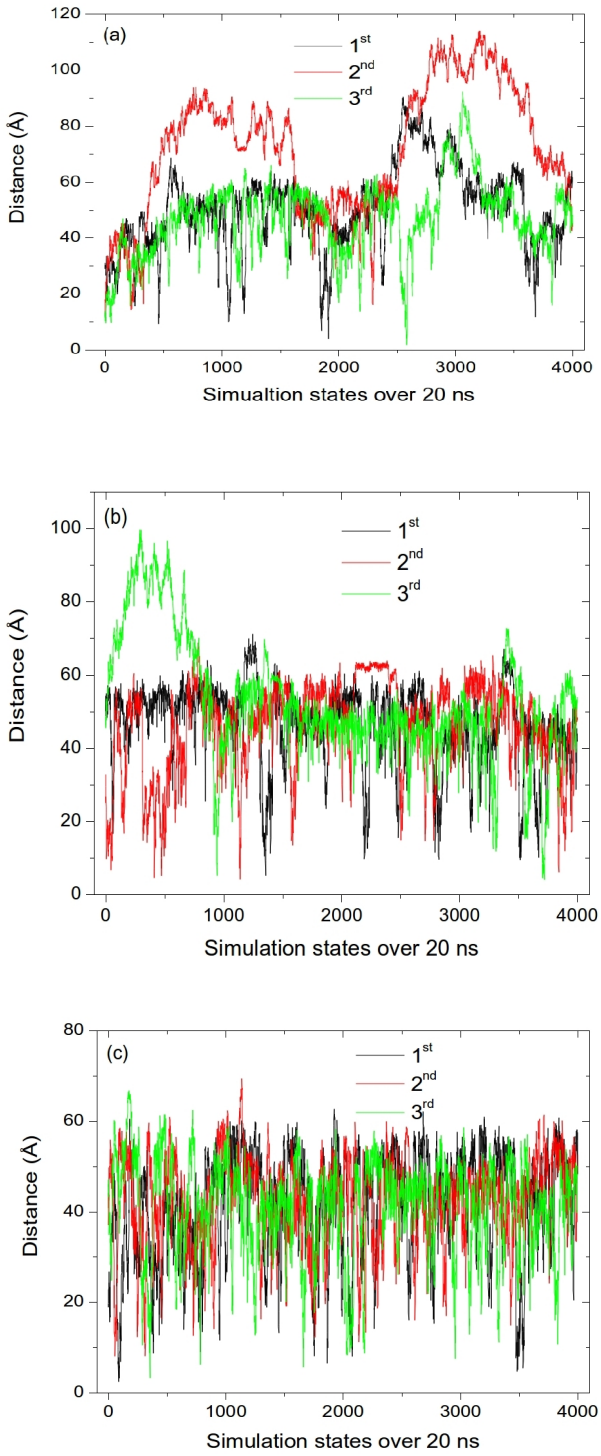

Figure 11. Representative dynamic displacement of CO_2 (a), N_2 (b) and O2 (c) molecules during the simulation time that are on the surface of the nano-bubbles at the end of the simulation. The displacement was computed with reference to the centre of the bubbles estimated at 20 ns time step. The three data sets in each plot (1^{st}, 2^{nd} and 3^{rd}) correspond to three distinct gas molecules.

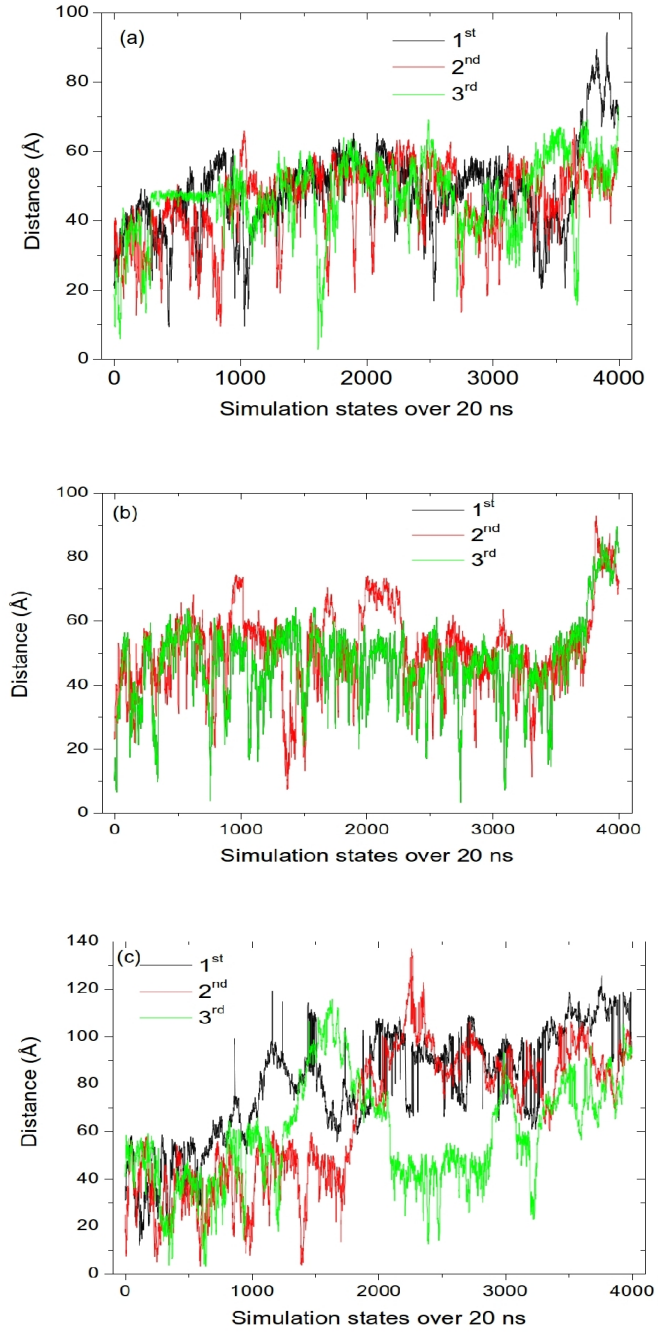

Figure 12. Representative dynamic displacement of CO_2 (a), N_2 (b) and O2 (c) molecules during the simulation time that are outside of the nano-bubbles at the end of the simulation. The displacement was computed with reference to the centre of the bubbles estimated at 20 ns time step. The three data sets in each plot (1^{st}, 2^{nd} and 3^{rd}) correspond to three distinct gas molecules.

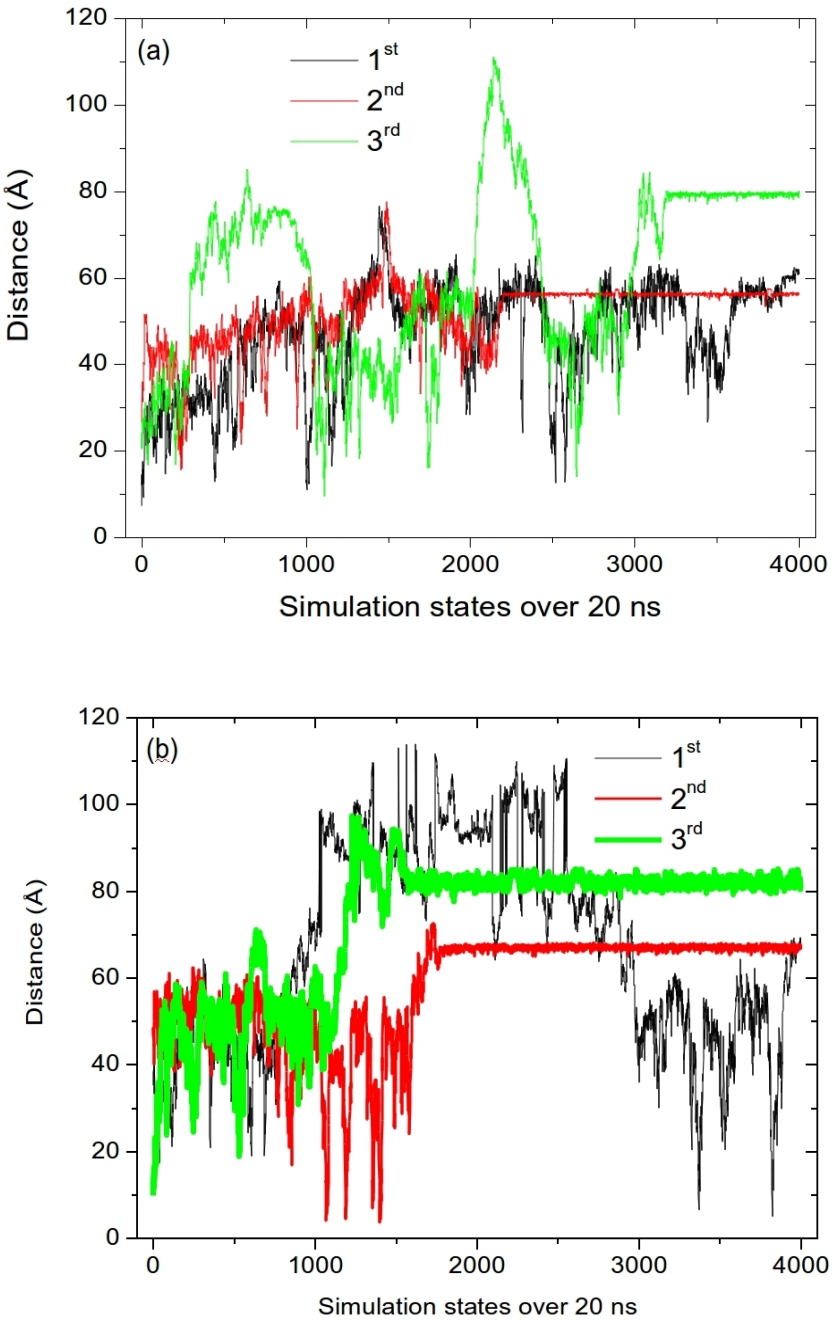

Figure 13. Representative dynamic displacement of CO_2 (a) and N_2 (b) during the simulation time and their attachment to the amorphous silica surface. The displacement was computed with reference to the centre of the bubbles estimated at 20 ns time step. The three data sets in each plot (1^{st}, 2^{nd} and 3^{rd}) correspond to three distinct gas molecules.

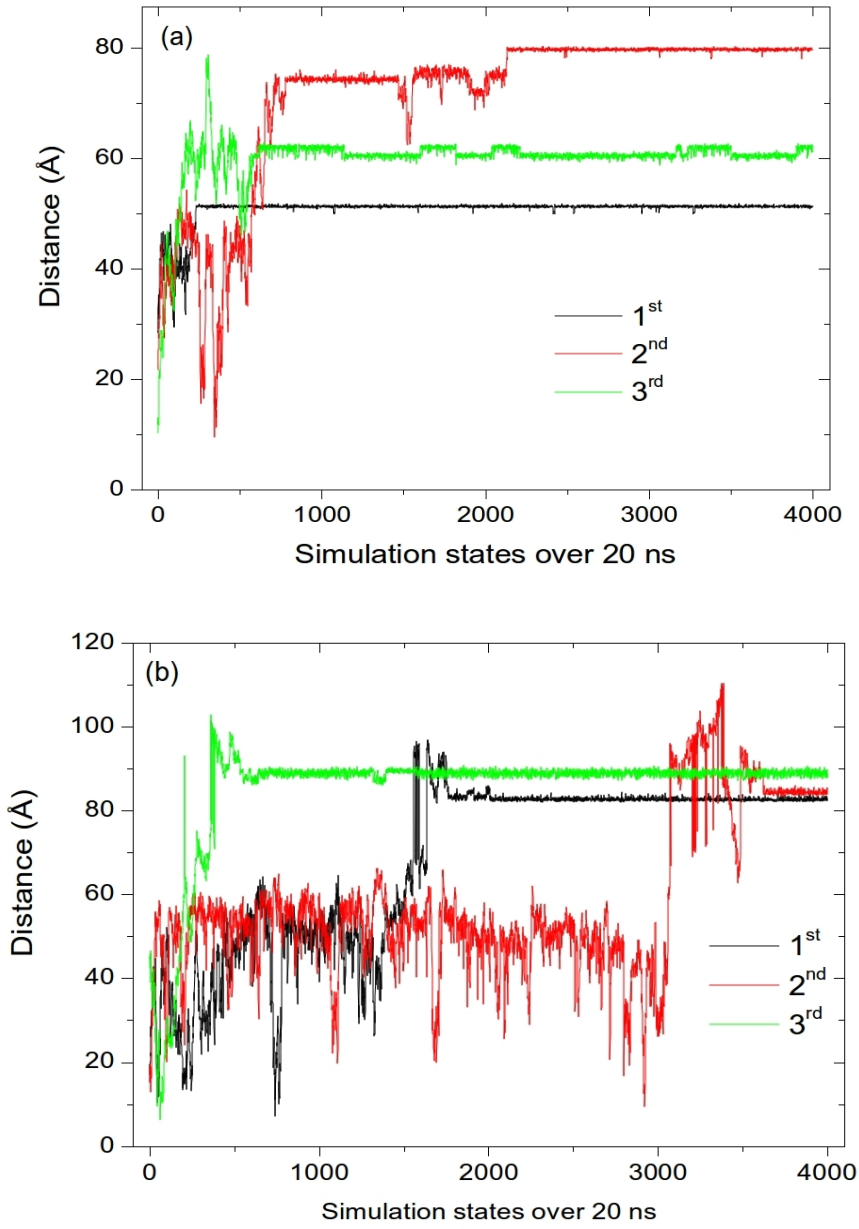

Figure 14. Representative dynamic displacement of CO_2 (a) and N_2 (b) during the simulation time and their diffusion and localisation in the amorphous silica matrix. The displacement was computed with reference to the centre of the bubbles estimated at 20 ns time step. The three data sets in each plot (1^{st}, 2^{nd} and 3^{rd}) correspond to three distinct gas molecules.